

Controllable Synthesis of Hierarchical Micro/Nano Structured FePO₄ Particles under Synergistic Effects of Ultrasound Irradiation and Impinging Stream

Bin Dong^{b,#}, Hongliang Qian^{b,#}, Chenyang Xue^a, Xiaogang Yang^{a,*}, Guang Li^{a,*}, George Z. Chen^{c,d}

^aDepartment of Mechanical, Materials and Manufacturing Engineering, The University of Nottingham Ningbo China, University Park, Ningbo 315100, P.R. China

^bDepartment of Pharmaceutical Engineering, School of Engineering, China Pharmaceutical University, Nanjing, 210009, China

^cDepartment of Chemical and Environmental Engineering, Faculty of Engineering, University of Nottingham, Nottingham NG7 2RD, United Kingdom

^dDepartment of Chemical and Environmental Engineering, The University of Nottingham Ningbo China, University Park, Ningbo 315100, P.R. China

Abstract

Hierarchical micro/nano-structured FePO₄ (FP) particles were environmental-friendly and controllable synthesized through synergistic intensification of ultrasound and impinging streams. Nano-scale FP seeds were firstly synthesized via ultrasound irradiation intensified impinging stream reaction (UISR), where the enhanced turbulent micromixing in the impinging streams benefits the nucleation process while the application of ultrasound to the impinging streams further intensifies such micromixing. The ultrasound frequency and power applied were 20 kHz and 600 W. The hierarchical micro/nano-structured FP particles are obtained when taking sufficient reaction time and stirring FP nano-seeds in a continuous stirring tank reactor (CSTR). Effects of the sonochemical pre-treatment, mean residence time and rotation speed on the physical-chemical properties of FP were investigated systematically. The characterization revealed that under the optimum operating condition, the FP particles presented near-spherical hierarchical micro/nano-structure, consisting of nanoscale primary grains. The mechano-chemical effects on the synthesized FP particles during different synthesis process were also studied.

Keywords: Micromixing; Fluid dynamics; Hierarchical micro/nano-structure; FePO₄; Mechano-chemical effects.

*Corresponding authors: Tel: +86-574-88180000 Ext: 8419 E-mail: Xiaogang.Yang@nottingham.edu.cn (XY); guang.li@nottingham.edu.cn

#Bin Dong and Hongliang Qian have contributed equally.

Nomenclature

Re	Reynolds number
d	hydraulic diameter (m)
u	mean velocity (m/s)
N_p	power number
n	rotation speed (rpm)
m	mass of solution (kg)
Da	impeller diameter (m)
P	power (W)

Greek letters

ε	turbulent dissipation rate (J/s·kg)
ρ	density of reactive solution (kg/m ³)
μ	viscosity (kg/(m·s))
ν_{ms}	kinematic viscosity of the mixed solution (Pa·s)
τ	turbulent shear stress (Pa)

1. Introduction

In recent years, mechanical force from fluid dynamic plays more important role in transferring energy to chemical bonds and driving chemical reactions during manufacturing process [1-3]. The chemical-physical properties and yield of as-synthesized products are significantly affected by local shear stress and micromixing intensity provided by fluid dynamics. In 2020, *Nature* reported that growth rate of crystals can be accelerated dramatically by local stirring rate and shear stress generated by fluid dynamics (physical effects) rather than surface-energy effects in classical Ostwald Ripening (chemical effects). Application of classical stirring method can influence the final size and quality of synthesized particles through modulating the shear rate, secondary nucleation and particle growth process [4]. *Cell* (2018) introduced that strong local shear stress generated by turbulence can promote the yield of platelet to enable clinical scale *ex vivo* manufacturing, which can not be achieved in laminar flow [5]. In terms of micromixing intensity, Liu et al. carried out that micromixing provided by different flow behavior (including laminar, vortex, and turbulent) influenced particle size, particle size

distribution, production rate, and reproducibility of core/shell nanocomposites (PTX@HF and SFN@HF) significantly [6,7]. Hu et al. developed turbulent mixing method in confined impinging jet device, and investigated how competition between micromixing time and assembly time adjusted size, composition, and *p*DNA payload of plasmid DNA/polycation complex nanoparticles [8]. Besides, it has been demonstrated that strong correlation is existed between local turbulent dissipation rate and physical properties of synthesized products. Both local shear stress and micromixing performance can be enhanced through increasing stirring rate [9].

The local shear stress and micromixing performance can be modulated by using hybrid reactor systems combined with different intensification method. Impinging streams has been recognized for a long time which can achieve very effective micromixing within an extremely short residence time when keeping the feeding rate steady [10,11]. Localized turbulent eddies and strong shear stress can be enhanced by violent collision between impinging streams [12]. In a synthesis process, efficient micromixing due to turbulent eddy motion can remarkably improve mass transfer rate among mixed solutions and increase reaction rate. Meanwhile, the local pressure fluctuations can also influence energy and mass transfer in the solution [13]. Furthermore, ultrasound-irradiation intensified synthesis method is a promising technology which can effectively enhance turbulence intensity and intensify the micromixing in the reactor so as to achieve the stronger turbulent shear stresses [14]. Such ultrasonic intensification can be applied in the industrial scale manufacturing process and material synthesis because of its fast, cost-effective and environmental-friendly features [15,16]. Ultrasound-intensified crystallization, or sonocrystallization, has shown to be able to improve crystal purity and product homogeneity, to shorten crystallization time and to enhance process stability [17,18]. When the liquid is irradiated by ultrasound, ultrasonic wave can induce acoustic cavitation and generate a large number of cavitation micro-bubbles. Instantaneous collapses of the cavitation micro-bubbles can create extremely high pressure (up to 1000 atm), temperature (up to 5000 K), and the heating/cooling rate (greater than $10^{10} \text{ K}\cdot\text{s}^{-1}$) in the cavitation zone, leading to the chemical and physical changes of the solution [19]. In addition, the application ultrasound irritation can help to prevent the agglomeration among particles and interaction between particles and reactor surface due to locally enhanced turbulence [20].

Iron (III) phosphate, or FePO_4 (FP), has been recognized as an appropriate and promising material, which is widely used in synthesis of the electrode precursor for lithium ion battery [21,22], in fabrication of catalyst [23,24], and in production of fertilizers [25]. According to previous studies, preparing FP particles with micro/nano hierarchical porous structure can improve FP performance, especially as precursor for lithium ion battery [26,27]. Some studies have successfully prepared FP particles with hierarchical structure. However, toxic chemicals (such as acetonitrile, tetrahydrofuran, etc.) are used as raw materials in these preparation processes, and this has posed potential risk to the researchers and environment [28-30]. So far, studies on green and controllable manufacturing of FP particles with hierarchical porous micro/nano structure are still rarely reported.

In the present study, FP particles of hierarchical micro/nano structure were prepared through inducing synergistic effect of impinging stream and ultrasound irradiation, instead of using additional toxic chemicals. Ultrasound-assisted impinging stream reaction (UISR) was used as pretreatment to enhanced mass transfer and nucleation rate and prepare FP nano-seeds. After that, FP particles with hierarchical micro/nano-structured morphology can be then obtained after taking enough reaction time and stirring the particles in a continuous stirring tank reaction (CSTR). The mechano-chemical effects of jointly applying ultrasound irradiation and impinging streams in the UISR, stirring rate and reaction time in CSTR on physical-chemical properties of synthesized FP particles were systematically assessed and discussed.

2. Synthesis and experimental methods

2.1 Synthesis of hierarchical micro/nano-structured FP

The schematic diagram to describe the synthesis process of hierarchical micro/nano-structured porous FP particles is shown in Figure 1. According to previous research, in the first step, $\text{Fe}(\text{NO}_3)_3 \cdot 9\text{H}_2\text{O}$ (99%) and $(\text{NH}_4)_2\text{HPO}_4$ (99%) were dissolved into DI water to prepare $\text{Fe}(\text{NO}_3)_3$ (1.0 mol L^{-1}) and $(\text{NH}_4)_2\text{HPO}_4$ (1.0 mol L^{-1}) aqueous solutions [31]. The pH value of $(\text{NH}_4)_2\text{HPO}_4$ was kept at required value through adding ammonia solution. FP seed-crystals were prepared through ultrasound-intensified impinging stream reaction (UISR). Two peristaltic pumps (BT100FJ, Baoding Chuangrui Ltd, China) were used to pump $\text{Fe}(\text{NO}_3)_3$ (500 mL, 1.0 mol L^{-1}) and $(\text{NH}_4)_2\text{HPO}_4$ (500 mL, 1.0 mol L^{-1}) aqueous solutions into two separate inlets of T-mixer at room temperature, while the flow rates were precisely controlled ($85.74 \text{ ml min}^{-1}$). In the meantime, the T-mixer was irradiated by applying an ultrasonic wave piezoelectric vibrator (600 W, 13 mm in diameter) with a resonance frequency of 20 kHz,

where the ultrasonic wave piezoelectric vibrator is inserted into an expanded chamber in the downstream of the T-junction. The pH value of mixed solution was kept at 1.80 by pH automatic controller through adding ammonia solution. All of the chemicals were purchased from Sinopharm Chemical Reagent Co., Ltd.

The nano-scale FP seed crystals were then immediately transferred into a continuous stirring tank reactor and stirred for up to 48 hours. The stirring system used in CSTR is a traditional mechanical stirrer with two impellers. The diameter and height of reactor is 28.4 cm and 12.2 cm, respectively. The radius of impeller is 2.5 cm. Four baffles (25.0×2.0×0.1 cm) are also placed in the continuous stirring reactor uniformly. The $\text{Fe}(\text{NO}_3)_3$ (1.0 mol L⁻¹), $(\text{NH}_4)_2\text{HPO}_4$ (1.0 mol L⁻¹) and NH_4OH (1.5 mol L⁻¹) aqueous solutions are continuously added into the reactor through three feeding tubes which are immersed in the solution. The solutions of $\text{Fe}(\text{NO}_3)_3$ (1.0 mol L⁻¹) and $(\text{NH}_4)_2\text{HPO}_4$ (1.0 mol L⁻¹) were continuously added into the reactor at a ratio of 1:1. Meanwhile, the continuous feeding rate of $\text{Fe}(\text{NO}_3)_3$ and $(\text{NH}_4)_2\text{HPO}_4$ aqueous solutions was precisely maintained at 0.86 ml min⁻¹ (1.0 rpm) for 48 hours. $\text{NH}_3\cdot\text{H}_2\text{O}$ solution (1.5 mol L⁻¹) was pumped into the reactor and carefully maintained the pH value of solution at 1.80. Around 400 mL of ammonia solution was used in 48 hours. During the test, the temperature was kept at 60 °C. FP samples were synthesized under the precisely controlled reaction time (12, 24, 36, 48 hours) and stirring rate ($n = 400, 800, 1200$ and 1600 rpm) to investigate the effects of mean residence time and stirring rate. The excess mixed solution will flow out of the reactor through the outlet tube which is placed on the side of the reactor. After 48 hours, the volume of the mixed solution is measured by a volumetric cylinder (1.0 L). The result shows that the maximum volume of solution is around 4.8 L during continuous stirring. Furthermore, for comparison purposes, FP samples were also synthesized by a conventional co-precipitation method in CSTR. $\text{Fe}(\text{NO}_3)_3$ (1.0 mol L⁻¹) and $(\text{NH}_4)_2\text{HPO}_4$ (1.0 mol L⁻¹) solutions were added continuously into the same CSTR with precisely controlled parameters. The pH value, temperature, stirring rate, and volumetric feeding rate were kept at the same level with the combined UISR and CSTR method.

The particle samples obtained by these two methods were subsequently washed with DI water for three times. After that, the slurry was filtered and dried at 100 °C for 12 hours. The samples were then calcined in the air at 600 °C for 10 hours to obtain anhydrous crystalline FP samples.

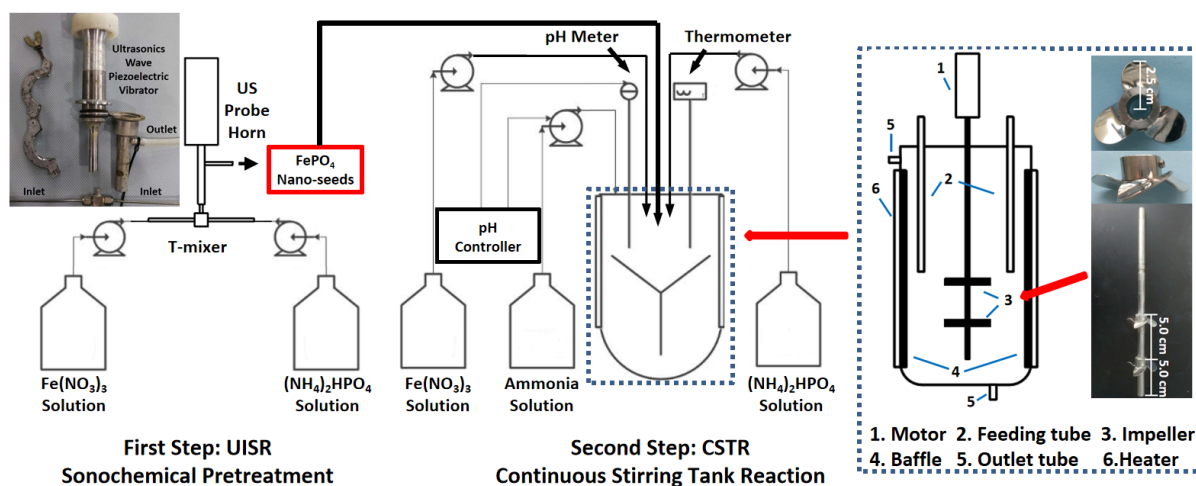


Figure 1. Schematic diagram of synthesis process.

2.2 Characterization

The crystal structure of as-synthesized samples were determined by a Bruker D8 series X-ray diffraction using Cu K α radiation ($\lambda=1.5406\text{\AA}$) operated at 40 kV and 40 mA. Morphology of the FP particles was measured by TEM (Tecnai F20, FEI, U.S) and SEM (Sigma VP, ZEISS, Germany). Brunauer Emmett Teller (BET, Micromeritics ASAP 2020, U.S.A) was used to analyse the porosity and surface area. Thermalgravimetric was measured by simultaneous Thermal Analyser (TG, NETZSCH STA 449 F3 Jupiter, Germany) at a heating rate of 10 °C/min in N₂. The particle size and distribution of the FP were determined by laser diffraction method (Mastersizer 3000, Malvern Inc, UK). According to previous research, ImageJ software was employed for the determination of FP primary grain size and distribution based on the SEM and TEM images [32]. For each sample, the diameter of more than 100 FP primary grains was calculated and analyzed to give out the average primary grain size.

3. Results and Discussion

3.1 Effect of UISR pretreatment on physico-chemical properties of FP samples

The synergistic effects of ultrasound irradiation and turbulent shear in impinging stream on particle morphology was investigated when mean residence time and post treatment stirring rate were maintained at 36 h and 1600 rpm, respectively. The SEM, TEM images and particle size distribution of as-synthesized particles are shown in Figure 2. As shown in Figure 2a, the FP particles prepared by conventional method (FP-Co) exhibit lower porosity and near-spherical shape with broader particle size distribution. The average secondary particle size and primary grain size are 2.47 μm and 258.8 ± 84 nm, respectively. As can be seen from Figure

2b and 2c, hierarchical micro/nano FP particles (FP-UI) can be well synthesized by using combination of UISR and CSTR. The micro-scale near-spherical secondary structure of the FP-UI has an average particle size of $1.75 \mu\text{m}$, consisting of nanospheres with diameter around $115.5 \pm 34 \text{ nm}$. In addition, three peaks can be observed in Figure 2d. The first peak ($0.45 \mu\text{m}$) can be attributed to the new-generated FP particles, while peak 3 are caused by the agglomeration of particles.

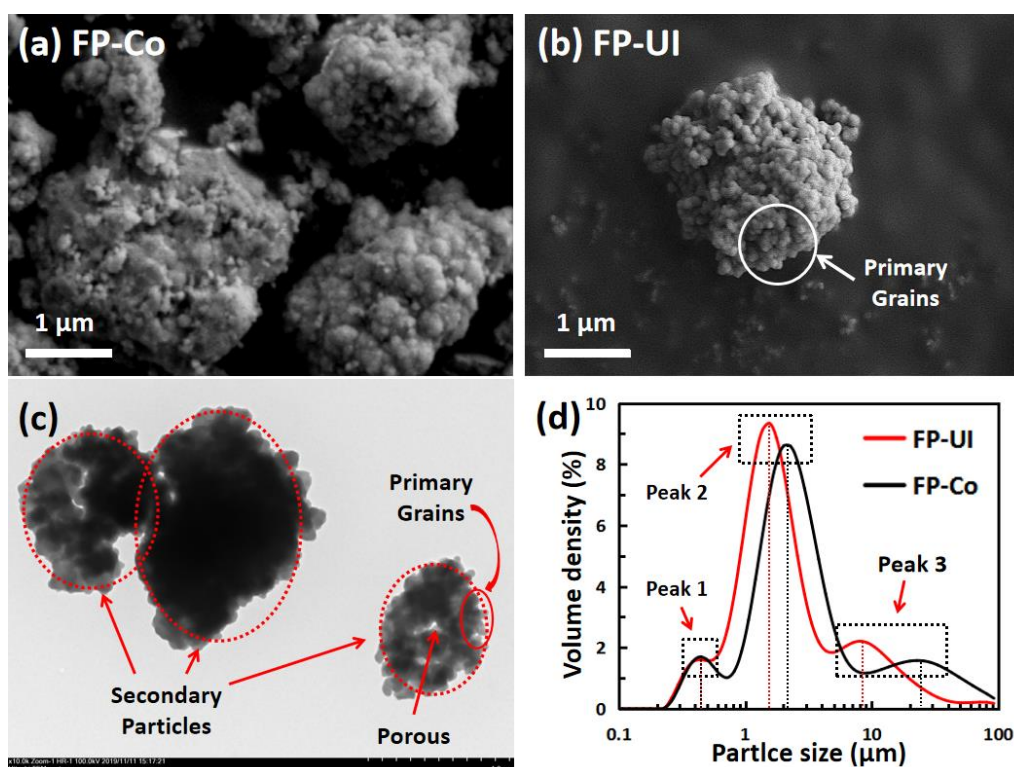


Figure 2. (a-b) SEM images of as-synthesized samples; (c) TEM image of FP-UI; (d) Particle size distribution of FP-UI and FP-Co.

The thermal properties of FP-UI was confirmed by TG-DTA at a heating rate of $10 \text{ }^\circ\text{C}$ in N_2 (Figure 3a). There is a strong endothermic peak around $130 \text{ }^\circ\text{C}$, and 19 % of sample weight is lost from $50 \text{ }^\circ\text{C}$ to $450 \text{ }^\circ\text{C}$, indicating the loss of crystal water and transformation of $\text{FePO}_4 \cdot x\text{H}_2\text{O}$ to anhydrous hexagonal FP. Moreover, x is calculated and found to equal 2, which is consistent with the theoretical value. The XRD patterns of as-synthesized samples are shown in Figure 3b and 3c. The XRD results of FP-UI and FP-Co samples, which are calcinated at $600 \text{ }^\circ\text{C}$ for 10 hours, match well with anhydrous hexagonal structure FP (JCPDS card No. 29-0715, $a = 5.035 \text{ \AA}$, $b = 5.035 \text{ \AA}$, $c = 11.245 \text{ \AA}$), suggesting the formation of perfect crystalline FP after calcination. The BET specific surface area and pore size distribution of the FP-UI and FP-Co samples have been characterized by N_2 adsorption-desorption analysis. The measured BET surface areas for FP-UI and FP-Co correspond to 18.65 and $8.59 \text{ m}^2/\text{g}$, respectively. As

shown in Figure 3c, the N₂ adsorption isotherm of FP-UI and FP-Co is Type III, which can be regarded as nonporous. However, as shown in Figure 3d, The pore area distribution based on desorption of both FP-UI and FP-Co samples present the existing of mesoporous (> 2 nm and < 50 nm) and macropores (> 50 nm). The acquirement of higher specific surface area and pore volume of FP-UI can be attributed to the decreasing of average grain size and the increasing amount of mesopores and macropores, which are shown in Figure 2b and 2c.

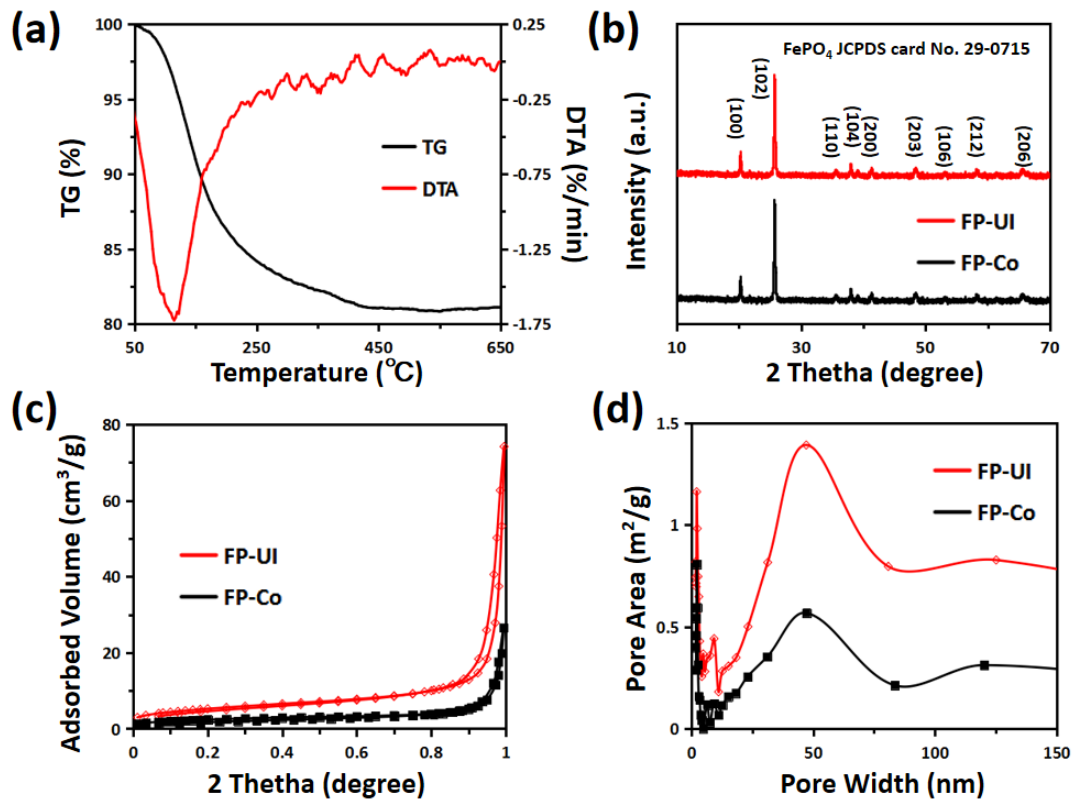


Figure 3. (a) TG-DTA curve of FP-UI; (b) X-ray diffraction patterns of FP; (c) N₂ adsorption-desorption isotherms of FP samples prepared by different methods; (d) Incremental pore area distribution.

3.2 Effect of reaction time and rotation speed in CSTR on physico-chemical properties of FP samples

To investigate the optimum reaction time, the experiments were conducted using different residence time by varying from 12 to 48 hours with a stirrer rotational speed of 1600 rpm. The SEM images of FP particles are shown in Figure 4(a-d). Besides, as the experiments were repeated for three times, the particle size distribution, and average size of primary grains and secondary particles are shown in Figure 4(e-f). There exists a clear trend that longer mean residence time of particles exposure to hydrodynamic fluid shear stress leads to more spherical morphology and narrower particle size distribution [33]. The co-precipitation process in the CSTR can be divided into two sub-processes, growth of core particles (heterogeneous

nucleation and particle growth) and homoagglomeration (homogeneous nucleation) of newly generated particles [34]. As the objective of the present work is to synthesize FP particles with hierarchical micro/nano structure, it is crucial to facilitate the homo-agglomeration of FP particles. The change of FP morphology can be explained from two points: decreasing of secondary particle size and increasing of primary grain size. When the mean residence time is 12 hours, most of the FP particles are nanoscale and agglomerated together randomly (see Figure 6a). Therefore, FP-12 sample exhibits larger average particle size (8.02 μm) and broader particle size distribution. The D_{x10} and D_{x90} value of the FP-12 particles are found to be 1.11 and 28.9 μm . The larger FP particles may be generated through the heterogeneous nucleation and particle growth processes of initial nanoscale FP seeds, while the smaller FP particles might be generated by homogeneous nucleation through the continuous precipitation in the CSTR. After 24 hours, it can be clearly observed that large amount of nanoscale FP particles are agglomerated and formed micro-scale FP particles (see Figure 6b). The average particle size reduces to 2.19 μm (FP-24). However, these particles are still broadly distributed. When increasing mean residence time to 36 hours, as shown in Figure 6c, more FP particles with near-spherical morphology and hierarchical micro/nano structure are generated. The average particle size of the FP further decreases to 1.75 μm , and the particle size distribution becomes much narrower. The values of D_{x10} and D_{x90} are 0.73 μm and 10.5 μm , respectively. It can be imagined that these newly generated FP particles play a role of “bridge” or “glue”, which consolidate the interactive connection among FP nano-seeds. After carrying out 48 hours of the experiment, the FP particles become larger and increasingly spherical, the average particle size has increased to 2.85 μm . However, the porous and hierarchical micro/nano structure cannot be observed due to the overgrowth of primary grains (Figure 6d). Thus, a longer exposure time to the hydrodynamic turbulent shear can contribute to the generation of FP particles with near-spherical shape and narrow particle size distribution. However, further increasing of mean residence time leads to the disappearance of porous structure.

In addition, the diameter of more than 100 primary grains was analyzed and calculated by ImageJ. According to Figure 6(a-d) and ImageJ analysis, the average primary grain size of the FP particles increases with increasing mean residence time. After 12 hours, the average primary grain size of the FP particles increases slightly to 137.0 nm (FP-12). As the continuous feeding of Fe^{3+} and PO_4^{3-} , the average primary grain size maintains an increasing tendency, improving from 164.6 nm (FP-24) to 176.4 nm (FP-36). When the mean residence time exceeds 36 hours,

the primary grains grow rapidly and the average grain size has attained 388.8 nm after 48 hours. This is the consequence of the newly generated FP nuclei aggregated to the surface of the early generated FP particles in the continuous reaction. It can be postulated that several primary grains combine together and overgrowth to yield a larger primary grain. Therefore, it is important to precisely control mean residence time for the green and controllable manufacturing of materials with hierarchical micro/nano structure. Based on the observations, it seems that 36 hours is the optimum mean residence time, because the FP-36 particles can present the nearly spherical morphology, most narrow particle size distribution, nano-scale primary grain, smallest average secondary particle size, and hierarchical micro/nano structure.

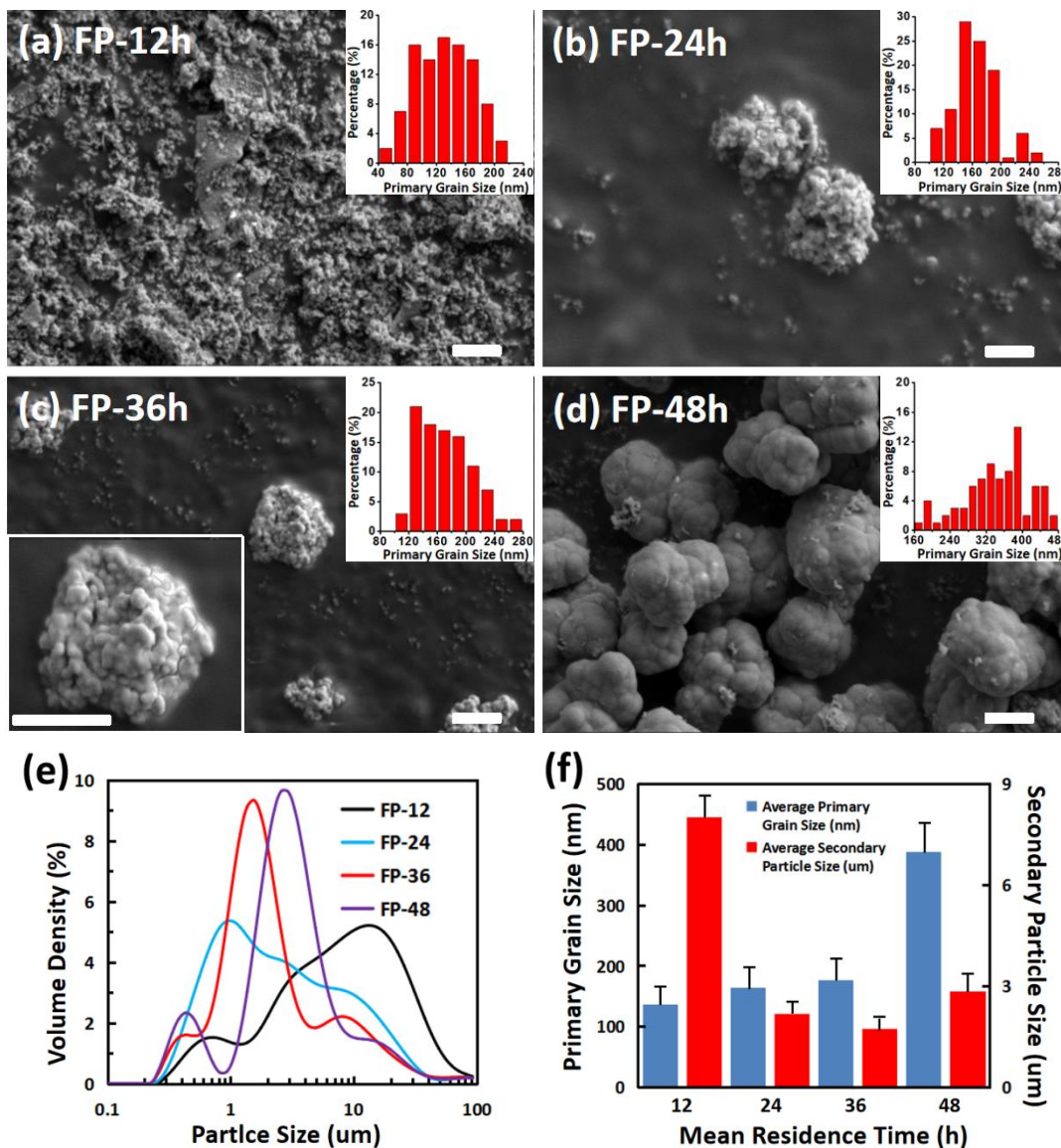


Figure 4. (a-d) SEM images of FP particles (scale bar: 1 μm); (e) Particle size distribution; (f) Average primary grain size and secondary particle size of FP sample synthesized with different mean residence time.

The influence of the turbulent shear on the FP samples in CSTR were evaluated at four different stirring rotational speeds, ranging from 400 to 1600 rpm. The SEM images and particle size distribution results of FP samples prepared at four different rotational speeds were shown in Figure 5. All the particles are composed of a larger number of densely aggregated nano-scale primary grains with spherical morphology. As expected, the SEM analysis also indicates that increasing of rotational speed can promote the particle sphericity and reduce the particle size of as-prepared FP samples. At low stirring rate, ($n = 400$ rpm), the as-prepared FP sample shows irregular particle shape with a broad particle size distribution. As the stirring rate increases to 1600 rpm, uniformly near-spherical FP particles are generated with a mean residence time of 36 hours. It can be seen clearly that the particle shape became spherical and the particle size distribution became narrower when increasing the rotational speed from 400 rpm to 1600 rpm.

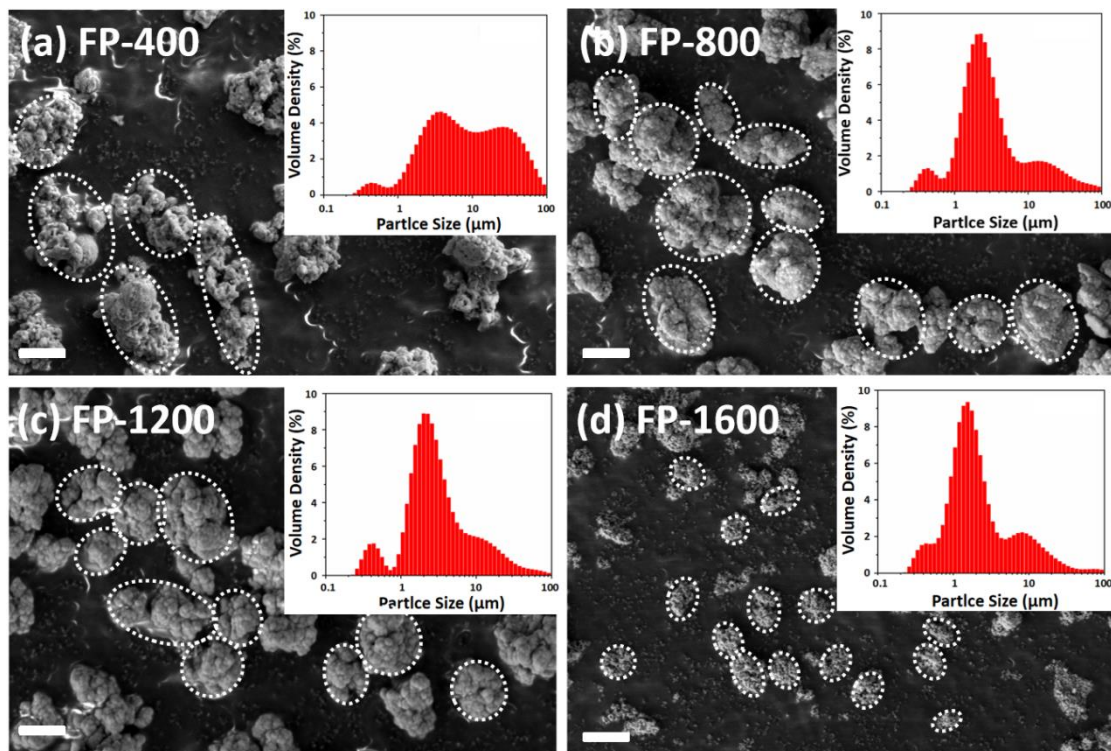


Figure 5. SEM images and particle size distribution of FP particles synthesized by different stirring rate (scale bar: 2 μm).

3.3 Formation mechanism of hierarchical micro/nano-structured FP particles

Due to the same reaction condition in CSTR, the generation of hierarchical micro/nano-structured FP particles can be attributed to the mechano-chemical effects of sonochemical pretreatment, especially synergistic effect between ultrasound and impinging stream. The SEM and TEM images of nanoscale FP seeds obtained by sonochemical pretreatment in UISR are

shown in Figure 6(a-c), while the formation mechanisms of FP nano-seeds in UITR and micro/nano structured particles in CSTR are schematically shown in Figure 6d and 6e. Large amount of spherical FP nano-seeds ranging from 20 to 80 nm can be generated after sonochemical pretreatment. In contrast, our previous study has demonstrated that the FP seeds produced by only impinging stream reaction and conventional co-precipitation method exhibited irregular morphology and larger size [31].

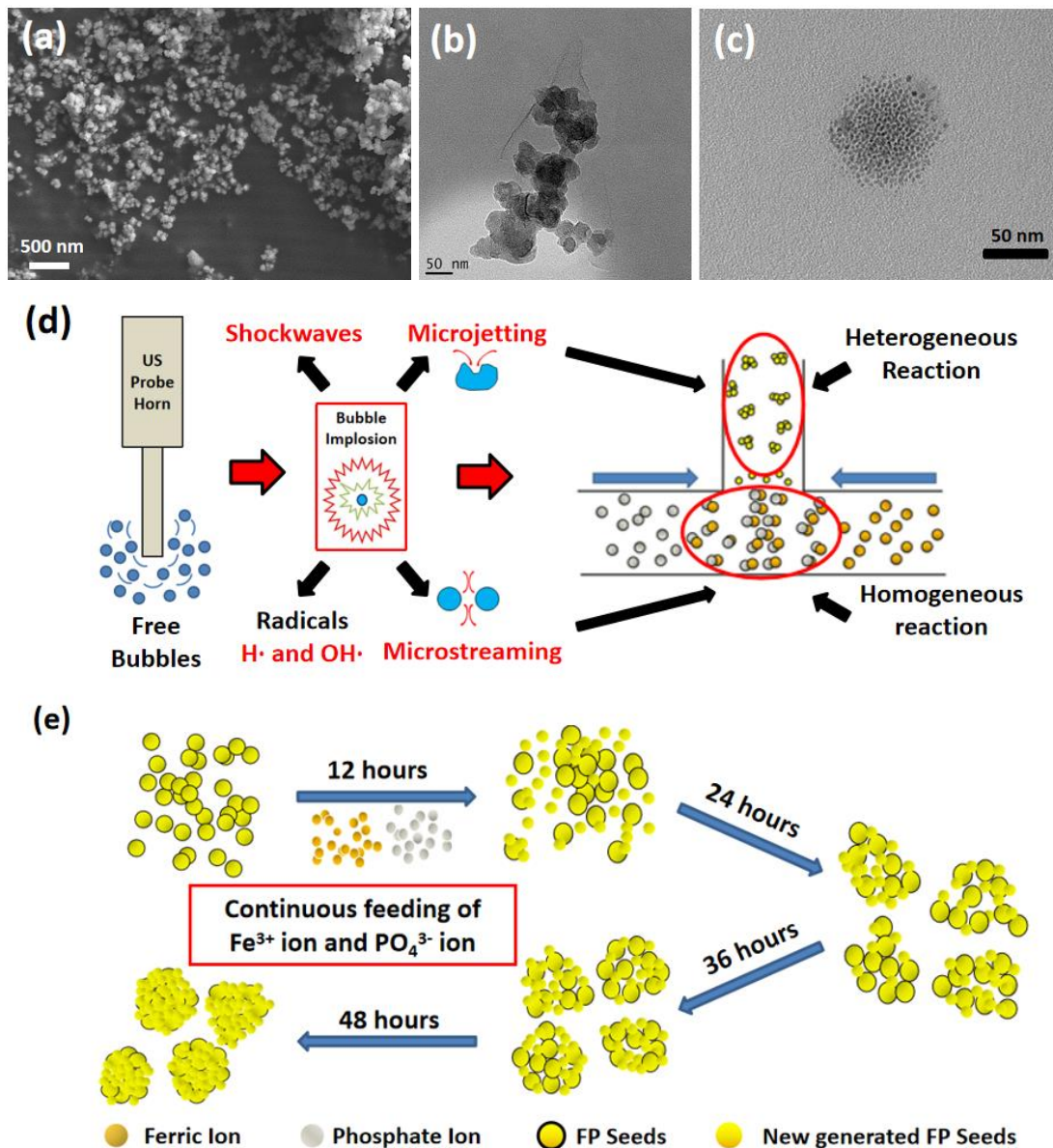


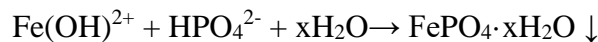
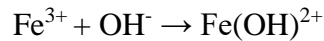
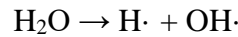
Figure 6. (a) SEM and (b-c) TEM images of FP nano-seeds; (d) schematic diagram of sonochemical pretreatment (UISR); (e) schematic diagram of hierarchical micro/nano-structured FP fabrication process.

As illustrated in Figure 5d, during UISR pretreatment, the Reynolds number (Re_{UISR}) for the impinging stream can be defined as:

$$Re_{UISR} = \frac{\rho u d}{\mu} \quad (1)$$

where u is the mean velocity in the inlet of the T-shape junction and d is the hydraulic diameter of the circular tube inlet. The density (ρ) and viscosity (μ) of mixed solution are 1.144×10^3 kg/m³ and 1.005×10^{-3} Pa·s, respectively. The tube diameter (d) is 3.5×10^{-3} m. As a result, the Reynolds number is 1165 in UISR system when the volumetric feeding rate kept at 85.74 ml·min⁻¹, which can be regarded as laminar flow ($Re < 2000$). In addition, the streams of Fe³⁺ and PO₄³⁻ solutions counter-impinge each other directly in the T-junction central zone of the T-mixer. The impinging stream can generate small turbulent eddies, while ultrasound wave can induce sharp localized pressure reduction and acoustic streaming [35].

Meanwhile, OH· and H· radicals, which can produce secondary radical species and promote the reduction rate, are also generated through sonolysis of water during sonochemical pretreatment [36]. The main reactions in this stage are summarized below:



As large amount of micro-bubbles are generated and instantly collapsed by ultrasound irradiation in the mixed solution, the collapse of such micro bubbles generates local micro-jetting due to the filling for the cavities generated by bubble bursting from the surrounding solution. This significantly promotes sufficient mixing of raw solutions jointly with the assistance of high level of supersaturation. Apart from that, the chemical reaction rate and nucleation rate can be enhanced significantly as the local extremely high temperature point sources (up to 5000 K) caused by ultrasound irradiation. Consequently, large amount of FP nuclei can be generated in the solution in an extremely short time. Furthermore, micro-jetting can enhance turbulent shear stress, preventing from agglomeration among the particles and circumventing the clogging on the internal walls of guided tubes and flow channels of the T-

mixer. Therefore, the synergistic effect of impinging stream and ultrasound results in the generation of highly turbulent in UISR, which intensified reactant mixing and facilitated nucleation to form FP nanoseeds.

After sonochemical pretreatment, FP nano-seeds are transferred into CSTR immediately, and hierarchical micro/nano-structured FP particles can be generated when FP-seeds take enough reaction time and stirring through particle growth and agglomeration in CSTR (Figure 6e). The results can be explained by comparison of the turbulent shear stress, turbulent dissipation energy, and the physical interactive force for the particles in the CSTR, synthesized at different stirring rate.

To assess the turbulent mixing effect in the CSTR, the turbulent dissipation energy per unit mass ε [J/s·kg] [37] can be estimated by

$$\varepsilon \propto \frac{N_p n^3 Da^5 \rho}{m} \quad (2)$$

where Da is the impeller diameter, n is the rotational speed (rpm), ρ is the density of reactive solution, m is the mass of solution hosted in the reactor and N_p is the power number. The Reynolds numbers and power number N_p can be defined as

$$Re_{CSTR} = \frac{\rho n Da^2}{60\mu} \quad (3)$$

$$N_p = \frac{P}{\rho n^3 Da^5} \quad (4)$$

where μ is the solution viscosity and P is the power. Based on the turbulent dissipation energy, turbulent shear stress τ , which is one of the most important characteristics of the turbulent mixing, can be estimated as

$$\tau = \mu \left(\frac{\varepsilon}{\nu_{ms}} \right)^{1/2} \quad (5)$$

where ν_{ms} is the kinematic viscosity of the mixed solution.

An increase in the rotational speed will enhance the turbulent energy dissipation rate and turbulent shear stresses. The turbulent shear stress τ influences the breakage/re-dispersion process of the aggregated particles in the CSTR. As a result, the mass transfer rate of formed particle nucleation, as well as the collision rate of the particle nuclei are increased. At a low rotational speed of 400 rpm (6.7 rps), the shear stress is likely weaker than the interactive force

among the aggregated primary grains, resulting in larger particle size and broader particle size distribution. With increasing the rotational speed to 1600 rpm (26.7 rps), the shear stress increases and overcomes physical interactive force acting on the particles. Then breakage and re-dispersion become dominated process and inhibit agglomeration. As a result, the particle morphology becomes spherical with decreased average particle size and narrowed particle size distribution.

4. Conclusions

In this work, hierarchical micro/nano-structured FP samples were synthesized through application of ultrasound irradiation and impinging streams in the UISR, precisely control mean residence time and modulation of the stirring rate in the CSTR. It has been revealed that ultrasound irradiation and impinging stream intensified micromixing together with post stirring in CSTR is promising controllable synthesis method for the preparation of hierarchical micro/nano-structured FP used in many fields. The conclusions reached from the present study can be summarized as follows:

(1) The application of synergistic effects between ultrasound and impinging stream leads to the generation of FP nano-seeds. Besides, precisely controlled mean residence time and stirring rate result in the decreasing of primary gains size and secondary particle size, and reduction in the spread of the particle size distribution. Extra-increase in the mean residence time has a negative impact. Consequently, both primary grain size and secondary particle size increase dramatically, and porous structure disappears when the mean residence time exceeds 36 hours.

(2) By adopting the sonochemical seed-mediated method, an increase in the rotational speed of the stirrer in the mixing tank can effectively reduce the spread of particle size distribution and improve sphericity of FP particles because the enhanced turbulent shear can facilitate the particle breakage and re-dispersion process.

(3) The reaction time in this study is relatively long and may consume more energy. However, no toxic additional chemicals are used in this method. Therefore, the combination of this method with renewable energy (such as solar energy) has potential for green and controllable synthesis of functional particle material with desired hierarchical micro/nano-structure by controlling fluid dynamics in the synthesis process and adjusting of mechano-chemical effects.

Acknowledgement

This work was supported by National Natural Science Foundation of China (NSFC) (Grant Nos. 21576141, 91534118), Zhejiang Provincial Natural Science Foundation (Grant No. LY15B060001), Natural Science Foundation of Jiangsu Province (Grant No. BK20190567) and the Fundamental Research Funds for the Central Universities (Grant No. 3011900170). This work was carried out at the International Doctoral Innovation Centre (IDIC).

References

1. W.F. Niamh, R. Etienne, A. Talal, R. Daly, Polymer mechanochemistry: manufacturing is now a force to be reckoned with. *Chem.* 4 (11) (2018) 2499-2537.
2. L. Takacs, The historical development of mechanochemistry. *Chem. Soc. Rev.* 42 (18) (2013) 7649-7659.
3. E. Boldyreva, Mechanochemistry of inorganic and organic systems: what is similar, what is different? *Chem. Soc. Rev.* 42 (18) (2013) 7719-7738.
4. J.K. Sun, Y.I. Sobolev, W. Zhang, Q. Zhuang, B.A. Grzybowski, Enhancing crystal growth using polyelectrolyte solutions and shear flow. *Nature* 579 (2020) 73-79.
5. Y. Ito, S. Nakanura, N. Sugimoto, T. Shigemori, Y. Kato, M. Ohno, S. Sakuma, K. Ito, H. Kumon, H. Hirose, H. Okamoto, M. Nogawa, M. Iwasaki, S. Kihara, K. Fujio, T. Matsumoto, N. Higashi, K. Hashimoto, A. Sawaguchi, K. Harimoto, M. Nakagawa, T. Yamamoto, M. Handa, N. Watanabe, E. Nishi, F. Arai, S. Nishimura, K. Eto, Turbulence Activates Platelet Biogenesis to Enable Clinical Scale Ex Vivo Production. *Cell* 174 (3) (2018) 636-648.
6. D. Liu, H. Zhang, S. Cito, J. Fan, E. Makila, J. Salonen, J. Hirvonen, T.M. Sikanen, D.A. Weitz, H.A. Santos, Core/shell nanocomposites produced by superfast sequential microfluidic nanoprecipitation. *Nano Lett.* 17 (2) (2017) 606-614.
7. D. Liu, H. Zhang, F. Fontana, J.T. Hirvonen, H.A. Santos, Current developments and applications of microfluidic technology toward clinical translation of nanomedicines. *Adv. Drug Deliver. Rev.* 128 (2018) 54-83.

8. Y. Hu, Z. He, Y. Hao, L. Gong, M. Pang, G.P. Howard, H.H. Ahn, M. Brummet, K. Chen, H. Liu, X. Ke, J. Zhu, C.F. Anderson, H. Cui, C.G. Ullman, C.A. Carrington, M.G. Pomper, J.H. Seo, R. Mittal, I. Minn, H.Q. Mao, Kinetic control in assembly of plasmid DNA/polycation complex nanoparticles. *ACS Nano* 13 (9) (2019) 10161-10178
9. L. Liu, X.G. Yang, G. Li, X.N. Haung, C.Y. Xue, Shear controllable synthesis of barium sulfate particles using lobed inner cylinder Taylor-Couette flow reactor, *Adv. Powder Technol.* 31 (3) (2020) 1088-1099.
10. S.W. Siddiqui, W.A.F.W. Mohamad, M.F.M. Rozi, I.T. Norton, Continuous, High-Throughput Flash-Synthesis of Submicron Food Emulsions Using a Confined Impinging Jet Mixer: Effect of in Situ Turbulence, Sonication, and Small Surfactants. *Ind. Eng. Chem. Res.* 56 (44) (2017) 12833-12847.
11. S. Bhattacharya, S.M. Kresta, Surface Feed with Minimum by-Product Formation for Competitive Reactions. *Chem. Eng. Res. Des.* 82 (9) (2004) 1153-1160.
12. A. Brito, M. Dias, R.J. Santos, Fully resolved modelling and simulation of micromixing in confined impinging jets. *Chem. Eng. Sci.* 211 (2020).
13. Y. Huang, P. Wang, Y. Yuan, X. Ren, F. Yang, Synergistic degradation of chitosan by impinging stream and jet cavitation. *Ultrason. Sonochem.* 27 (2015) 592-601.
14. Y.Q. Guo, X.G. Yang, G. Li, B. Dong, L.M. Chen, Effect of ultrasonic intensification on synthesis of nano-sized particles with an impinging jet reactor, *Powder Technol.* 354 (2019) 218-230.
15. S. Nalesso, M.J. Bussemaker, R.P. Sear, M. Hodnett, J. Lee, A review on possible mechanisms of sonocrystallisation in solution. *Ultrason. Sonochem.* 57 (2019) 125-138.
16. G. Chatel, How sonochemistry contributes to green chemistry. *Ultrason. Sonochem.* 40 (2018) 117-122.
17. J. Lee, M. Ashokkumar, S.E. Kentish, Influence of mixing and ultrasound frequency on antisolvent crystallisation of sodium chloride. *Ultrason. Sonochem.* 21 (2014) 60-68.
18. S.K. Bhangu, M. Ashokkumar, J. Lee, Ultrasound assisted crystallization of paracetamol: crystal size distribution and polymorph control. *Cryst. Growth Des.* 16 (2016) 1934-1941.

19. W.B. McNamara, Y.T. Didenko, K.S. Suslick, Sonoluminescence temperatures during multi-bubble cavitation. *Nature* 401 (1999) 772-775.
20. D.F. Rivas, S. Kuhn, Synergy of microfluidics and ultrasound: process intensification challenges and opportunities. *Topics Curr. Chem.* 374 (2016) 70-99.
21. Q. Cui, C. Luo, G. Li, G. Wang, K. Yan, Environmentally friendly synthesis of LiFePO₄ using Fe–P waste slag and greenhouse gas CO₂. *Ind. Eng. Chem. Res.* 55 (26) (2016) 7069-7075.
22. S. Ye, E. Yasukawa, M. Song, A. Nomura, H. Kumakura, Y. Kubo, Solventless synthesis of core–shell LiFePO₄/carbon composite for lithium-ion battery cathodes by direct pyrolysis of coronene. *Ind. Eng. Chem. Res.* 57 (41) (2018) 13753-13758.
23. J. L. Zhu, J. Wang, C. Shan, J. Zhang, L. Lv, B. Pan, Durable activation of peroxymonosulfate mediated by Co-doped mesoporous FePO₄ via charge redistribution for atrazine degradation, *Chem. Eng. J.* 375 (2019) 122009-122018.
24. H. Huang, Y. Su, Z. Long, G. Chen, Y. Yao, Enhanced formation of 5-hydroxymethylfurfural from glucose using a silica-supported phosphate and iron phosphate heterogeneous catalyst, *Ind. Eng. Chem. Res.* 57 (31) (2017) 10198-10205.
25. D. Sega, G. Ciuffreda, G. Mariotto, B. Baldan, A. Zamboni, Z. Varanini, FePO₄ nanoparticles produced by an industrially scalable continuous-flow method are an available form of P and Fe for cucumber and maize plants, *Sci. Rep.* 9 (2019) 11252-11264.
26. M.S. Whittingham, Lithium Batteries and Cathode Materials. *Chem. Rev.* 104 (2004) 4271-4301.
27. K.X. Wang, X.H. Li, J.S. Chen, Surface and interface engineering of electrode materials for lithium-ion batteries. *Adv. Mater.* 27 (2015) 527-545.
28. Y.M. Wu, Z.H. Wen, J.H. Li, Hierarchical carbon-coated LiFePO₄ nanoplate microspheres with high electrochemical performance for Li-ion batteries. *Adv. Mater.* 23 (2011) 1126-1129.
29. Y.J. Fang, L.F. Xiao, J.F. Qian, X.P. Ai, H.X. Yang, Y.L. Cao, Mesoporous amorphous FePO₄ nanospheres as high-performance cathode material for sodium-ion batteries. *Nano Lett.* 14 (2014) 3539-3543.

30. C. Li, Z.Y. Guo, Y. Pang, Y.H. Sun, X.L. Su, Y.G. Wang, Y.Y. Xia, Three-dimensional ordered macroporous FePO₄ as high-efficiency catalyst for rechargeable Li–O₂ batteries. *ACS Appl. Mater. Inter.* 8 (2016) 31638-31645.
31. B. Dong, X.N. Huang, X.G. Yang, G. Li, L. Xia, G.Z. Chen, Rapid preparation of high electrochemical performance LiFePO₄/C composite cathode material with an ultrasonic-intensified micro-impinging jetting reactor, *Ultrason. Sonochem.* 39 (2017) 816-826.
32. X.L. Ren, K. Turchenuik, D. Lewis, W.B. Fu, A. Magasinski, M.W. Schauer, G. Yushin, Iron phosphate coated flexible carbon nanotube fabric as a multifunctional cathode for Na-Ion batteries, *Small* 14 (43) (2018) 1703425-1703433.
33. D.K. Thai, Q.P. Mayra, W.S. Kim, Agglomeration of Ni-rich hydroxide crystals in Taylor vortex flow. *Powder Technol.* 274 (2015) 5-13.
34. J.E. Kim, W.S. Kim, Synthesis of core-shell particles of nickel-manganese-cobalt hydroxides in a continuous couette-taylor crystallizer. *Cryst. Growth Des.* 17 (2017) 3677-3686.
35. M. Rahimi, B. Aghel, B. Hatamifar, M. Akbari, A. Alsairafifi, CFD modeling of mixing intensification assisted with ultrasound wave in a T-type microreactor, *Chem. Eng. Process. Process Intensif.* 86 (2014) 36-46.
36. J.H. Bang, K.S. Suslick, Applications of ultrasound to the synthesis of nanostructured materials, *Adv. Mater.* 22 (2010) 1039-1059.
37. M.H. Sung, I.S. Choi, J.S. Kim, W.S. Kim, Agglomeration of yttrium oxalate particles produced by reaction precipitation in semi-batch reactor. *Chem. Eng. Sci.* 55 (2000) 2173-2184.